Surface Science 256 (1991) 385–396
North-Holland

Calculation of ion scattering yields from simulated crystal surfaces: theory and application to melting and non-melting Al surfaces

A.W. Denier van der Gon, D. Frenkel, J.W.M. Frenken
FOM-Institute for Atomic and Molecular Physics, Kruislaan 407, 1098 SJ Amsterdam, Netherlands

R.J. Smith
Physics Department, Montana State University, Bozeman, MT 59717, USA

and

P. Stoltze
Technical University of Denmark, DK 2800 Lyngby, Denmark

Received 19 December 1990; accepted for publication 3 April 1991

We present a formalism for the calculation of medium-energy ion scattering yields from crystal surfaces that are simulated using the Monte Carlo or molecular-dynamics method. Input in the calculations is the interatomic potential of the atoms in the crystal and the ion–atom interaction potential. We have applied the formalism to calculate scattering yields from Al(111) and Al(110) surfaces. In these simulations the effective-medium theory is used to describe the interactions between the Al atoms. The results of the calculation are compared with experimental scattering yields. Excellent agreement is obtained at low temperatures, where both surfaces are ordered, as well as at temperatures close to the bulk melting point, where the Al(110) surface exhibits surface melting.

1. Introduction

Computer simulations of crystal surfaces employing the molecular-dynamics (MD) and Monte Carlo (MC) methods have developed into an important tool for studying the structure, dynamics and phase transitions of surfaces. The computing power presently available allows for simulations of surfaces based on complicated and supposedly "realistic" Hamiltonians, as has been demonstrated for, e.g., Si, Ge, Cu, Au, Al and Ni [1–13]. How realistic the description of the interactions actually is can be judged only from detailed comparisons with experimental observations on the corresponding real systems. Ideally, one would like to simulate the outcome of specific surface experiments, integrated over a large number of MD time steps, or, alternatively, averaged over a large number of independent MC atomic configurations. For surfaces a quantitative direct comparison is only rarely made because of the complexity of a sufficiently sophisticated simulation of most relevant surface-sensitive experimental techniques.

In this paper we show how to calculate medium-energy ion scattering yields from simulated crystal surfaces. Medium-energy ion scattering (MEIS) is a sensitive tool for the determination of the structure, morphology and composition of clean and adsorbate- or overlayer-covered surfaces [14]. MEIS is also used to study melting and nonmelting of crystal surfaces [15–17]. Calcu-

lational methods for the simulation of ion scattering experiments have been developed before [18–21], but the applications have been limited to ordered surfaces in which the atoms occupy well-defined positions and are assumed to vibrate according to simple (usually Gaussian) probability distributions.

The scheme we present here is designed to compute scattering yields from crystal surfaces that are simulated by the MC method. We use the MC technique to generate "snapshots" of the atomic configuration in a unit cell of the crystal according to a particular many-body Hamiltonian. Subsequently, ion scattering yields are calculated for each snapshot and averaged over all snapshots. In this method, correlations of the atomic vibrations, non-Gaussian displacement distributions, and possible disorder in the surface region are taken into account in a natural way, as they are determined completely by the interatomic potential used in the MC simulations. The ion–atom scattering potentials are known rather accurately and have been tested extensively for well-ordered surfaces. Consequently, the scattering yields resulting from our MC simulations can be compared quantitatively, *on an absolute scale*, with the experimental yields from real crystal surfaces. This provides us with a sensitive test of the adequacy of the Hamiltonian in the simulations.

In section 2 we present the general formalism for the calculation of ion scattering yields, and discuss in detail where the new approach differs from the conventional methods. We have applied our new method to Al(111) and Al(110) surfaces. In these simulations we employ the effective-medium theory (EMT) to describe the interactions between the Al atoms [22]. The EMT is discussed briefly in section 3 and all equations needed to evaluate the total energy of a system of Al atoms are given explicitly. Details of the configurations used in the MC simulations and the ion scattering calculations are also described in section 3. The results are presented in section 4 and compared with experimental scattering yields. Further analysis of the simulation results in section 5 reveals a shortcoming of the periodic boundary conditions that are generally used in MC and MD simulations. Finally, we show that the onset of surface melting of Al(110), as seen with ion scattering, is accompanied by the creation of adatoms and vacancies.

2. Theory

Consider an ion beam impinging on a canonical ensemble of N atoms with the coordinates of atom i given by $\boldsymbol{x}_i$. Let $\boldsymbol{X}$ denote a specific combination $\{\boldsymbol{x}_i;\ i=1,\ N\}$. The total normalized scattering yield from the system is the scattering probability per atom $Y_i(\boldsymbol{e}^1,\ \boldsymbol{e}^2)$ summed over all atoms i. $Y_i(\boldsymbol{e}^1,\ \boldsymbol{e}^2)$ is defined as the average probability for ions impinging along direction $\boldsymbol{e}^1$ to reflect from atom i and to be detected in the direction $\boldsymbol{e}^2$, and is normalized such that it equals unity in the absence of shadowing and blocking effects [23]:

$$Y_i = Z^{-1}\int_{\Omega} F_i^1(\boldsymbol{e}^1,\ \boldsymbol{X})F_i^2(\boldsymbol{e}^2,\ \boldsymbol{X}) \times \exp\left[-H(\boldsymbol{X})/k_{\mathrm{B}}T\right]\ \mathrm{d}^3\boldsymbol{X}. \quad (1)$$

Here, F_i^1 is the normalized flux of impinging ions at position $\boldsymbol{x}_i$, F_i^2 is the normalized flux of ions able to reach the detector from $\boldsymbol{x}_i$. F_i^1 and F_i^2 are dimensionless scalars, normalized such that they equal unity in the absence of shadowing and blocking effects. $H(\boldsymbol{X})$ is the Hamiltonian of the N-atom system and Z denotes the corresponding partition function

$$Z = \int_{\Omega} \exp\left[-H(\boldsymbol{X})/k_{\mathrm{B}}T\right]\ \mathrm{d}^3\boldsymbol{X}. \quad (2)$$

Since the ions travel much faster than the atoms in the system, F_i^1 and F_i^2 are independent of the atomic momenta; the ions "see" instantaneous snapshots of the ensemble. For this reason the kinetic energy contribution to the total energy can be omitted from both H and Z, and H just represents the potential energy of the system. The integration is thus restricted to the integration volume Ω of all the spatial atom coordinates $\boldsymbol{X}$, as was already done in eqs. (1) and (2). In eq. (1) the scattering yield is calculated as a weighted average over all possible configurations $\boldsymbol{X}$ with a weight factor given by $\exp[-H(\boldsymbol{X})/k_{\mathrm{B}}T]$. In conven-

tional simulations of MEIS experiments the probability distribution of atoms to occupy positions x_i is modelled by a simple function of x_i. For example, in the majority of simulations the atoms are assumed to form a harmonic lattice, and to vibrate according to Gaussian distributions centred around the equilibrium lattice sites. In that case, the weight factor $\exp[-H(X)/k_BT]$ reduces to the probability density

$$\prod_{i=1}^{N} G_i(x_i),$$

where G_i is the Gaussian probability density for atom i to occupy position x_i, which is normalized such that $Z = 1$. (The functions G_i may also be conditional probability distributions in order to model correlated vibrations [21,24].) We then recover eq. (2.1) of ref. [21]. Here, we concentrate on the general case where the position distributions of the atoms are not known a priori, but where the potential energy of the system is a known function of the atomic coordinates. This approach allows us to go beyond the case of simple harmonic crystals and to treat disordered systems as well.

Let us assume that H is a known function of the atomic coordinates x_i only. In section 3.1 we discuss in detail the H for a system of Al atoms. Using the Metropolis scheme we perform a MC simulation of the system and generate a total of M configurations, where each configuration has probability $\exp[-H(X)/k_BT]/Z$ to be generated [25]. The scattering probability of atom i is approximated by [25]:

$$Y_i \approx \frac{1}{M} \sum_{j=1}^{M} F_i^1\left(e^1, X_j\right) F_i^2\left(e^2, X_j\right). \tag{3}$$

The summation j runs over the M snapshots X_j generated by the Metropolis algorithm. The problem of calculating the scattering yields is now reduced to evaluating the fluxes $F_i^1(e^1, X_j)$ and $F_i^2(e^2, X_j)$ for each generated X_j. Time reversibility of the ion trajectories makes the flux $F_i^2(e^2, X_j)$ equivalent to $F_i^1(-e^2, X_j)$, which further reduces the problem to the calculation of incident ion fluxes only [21].

The flux F_i^1 is determined by numerical integration, i.e., by tracking a finite number of L^1 ions through the particular snapshot, each ion impinging at a different position x_0 in the surface plane. The tracking of ions through the snapshots follows the method described in ref. [21]. Briefly, the Molière potential [26] is used to calculate the deflection of an ion each time it passes an atom. To allow for an efficient search for possible collision partners of ions, the atoms in the snapshot are assigned to points of a virtual lattice [21]. In our simulations of ordered and melting Al surfaces we have simply taken a rectangular lattice which contains the extrapolated bulk Al lattice sites. Each atom is linked to the closest site on this lattice. In practice it never occurred that more than one atom was assigned to the same lattice point in this way. In the Al simulations, this method of searching for collision partners by use of the auxiliary lattice implies that all atoms within the distance of 0.7 Å from the ion track are recognised as possible collision partners. The atoms that are not considered deflect the ions less than 0.03°.

In order to efficiently calculate the flux F_i^1 we determine its average value over a microscopic volume around atom i. To this end we "blur" the instantaneous position x_i of the atom into a Gaussian distribution

$$G(r, x_i) = \frac{1}{(2\pi\delta^2)^{3/2}} \exp\left(-\frac{|r - x_i|^2}{2\delta^2}\right), \tag{4}$$

with $\int G(r, x_i)\, d^3r = 1$. Let $\bar{F}_i^1$ be the weighted average of F_i^1 over the distribution function G. If δ is chosen small enough, then $\bar{F}_i^1$ is a good approximation to F_i^1. The flux can thus be represented as

$$F_i^1(e^1, X) = \lim_{\delta \downarrow 0} \bar{F}_i^1(e^1, X) = \lim_{\delta \downarrow 0} \frac{1}{\Phi^1} \sum_{k^1=1}^{L^1} g_{k^1}(\xi_i). \tag{5}$$

Φ^1 is the flux of incoming ions in a plane perpendicular to e^1, and the summation k^1 runs over the L^1 impingement positions x_0. By $g_{k^1}(\xi_i)$ we denote the contribution of the k^1th ion trajectory

to the average flux around atom i. It is obtained by integration of $G(\boldsymbol{r}, \boldsymbol{x}_i)$ along the ion track:

$$g_{k^1}(\xi_i) = \int_{k^1} G(\boldsymbol{r}, \boldsymbol{x}_i)\, \mathrm{d}\boldsymbol{r} = \frac{1}{2\pi\delta^2}\exp\left(-\frac{\xi_i^2}{2\delta^2}\right), \tag{6}$$

where $\xi_i \equiv \xi_i(\boldsymbol{e}^1, \boldsymbol{x}_0, \boldsymbol{X})$ is the impact parameter of the k^1th ion with respect to the position $\boldsymbol{x}_i$ of atom i. Note, that our choice of a Gaussian form for the averaging function G is arbitrary. Other functional forms such as a uniform distribution within a sphere with radius δ would serve the averaging purpose equally well. For the scattering yield we finally arrive at

$$Y_i = \lim_{\delta \downarrow 0} \frac{1}{M\Phi^1\Phi^2} \sum_{j=1}^{M} \left\{ \sum_{k^1=1}^{L^1} g_{k^1}\left[\xi_i\left(\boldsymbol{e}^1, \boldsymbol{x}_0, \boldsymbol{X}_j\right)\right] \times \sum_{k^2=1}^{L^2} g_{k^2}\left[\xi_i\left(-\boldsymbol{e}^2, \boldsymbol{x}_0, \boldsymbol{X}_j\right)\right] \right\}. \tag{7}$$

In practice, δ has to be assigned a nonzero value smaller than the one-dimensional root-mean-square (rms) displacement of atoms at each given temperature. This follows from the consideration that for such choices the total energy of an atomic configuration does not change noticeably when one atom is displaced over a distance δ, and thus the resulting configuration has virtually the same probability to be generated by the Metropolis algorithm as the original configuration. In section 3.2 we comment further on the values used for δ.

3. Simulations of Al surfaces

3.1. Effective-medium theory

Input for the MC simulations described in the preceding section is an expression for the potential energy H of the system. In this study we have used the effective-medium theory to calculate the potential energy for a system of Al atoms. A detailed derivation of the EMT has been given by Jacobsen et al. [22]. It has been demonstrated that the EMT predicts both bulk properties of Al such as the cohesive energy, the lattice constant, the bulk modulus and the phonon dispersion curves, and surface properties such as the surface energy and the surface relaxations rather well [22]. The evaluation of the potential is efficient enough to be used for MC and MD simulations [6–8,27]. In the EMT the energy of each atom is determined by the average electron density at the position of the atom, caused by the surrounding atoms. The energy of an atom for a given electron density is taken from the calculation of embedding energies of an atom in a homogeneous electron gas. Here, we give a résumé of the expressions involved in the calculation of H:

$$H = \sum_{i=1}^{N} \left[E_c(\bar{n}_i) + \alpha\left(\bar{n}_i - \bar{n}_i^{\mathrm{fcc}}\right)\right]. \tag{8}$$

The function E_c in eq. (8) represents the contribution of atom i to the cohesive energy of the system, and depends on $\bar{n}_i$, which is the average electron density from the surrounding atoms over a neutral sphere around atom i, E_c may be expanded as

$$E_c(\bar{n}_i) = E_0 + E_2\left(\frac{\bar{n}_i}{n_0} - 1\right)^2 + E_3\left(\frac{\bar{n}_i}{n_0} - 1\right)^3. \tag{9}$$

Since the neutral spheres around the atoms may overlap or may not cover some regions at all, an electrostatic correction is needed which is approximated by the second term in eq. (8). The correction term is taken to vanish for a perfect fcc lattice. The average densities $\bar{n}_i$ and $\bar{n}_i^{\mathrm{fcc}}$ are calculated using

$$\bar{n}_i = n_0 \exp\left[-\eta(s_i - s_0)\right], \tag{10}$$

with

$$s_i = -\frac{1}{\beta\eta_2}\ln\left[\frac{1}{12\gamma_1}\sum_{j\neq i} W(r_{ij})\exp(-\eta_2 r_{ij})\right] \tag{11}$$

and

$$\bar{n}_i^{\mathrm{fcc}} = \frac{n_0}{12\gamma_2}\exp(\eta s_0)\sum_{j\neq i} W(r_{ij})\exp(-\eta r_{ij}/\beta). \tag{12}$$

The summation indices i and j run over all atoms in the system, and r_{ij} is the distance between

Table 1
Parameters used in the effective-medium theory for the simulation of Al surfaces (from ref. [22])

Parameter	Value
E_0 (eV)	−3.28
E_2 (eV)	1.12
E_3 (eV)	−0.35
n_0 (Å^{-3})	0.0473
α (eV Å^3)	189.49
η (Å^{-1})	3.781
η_2 (Å^{-1})	2.401
s_0 (Å)	1.587
β	$\frac{1}{2}\sqrt{2}(16\pi/3)^{1/3}$

atoms i and j. The values for the constants in eqs. (8)–(12) for Al were taken from ref. [22] and are given in table 1. The function $W(r_{ij})$ in eqs. (11) and (12) serves to cut off the interactions beyond a certain distance. The choice of a large cut-off radius is important for melting studies. In this study the cutoff was put between fourth- and fifth-nearest neighbours at a distance $R_c = [\sqrt{2} + \sqrt{(5/2)}]a(T)$, with $a(T)$ the temperature-dependent lattice constant. The function W is defined as

$$
\begin{aligned}
&W(r) = 1 \\
&\quad \text{for} \quad r \le R_c - \frac{2}{A}, \\
&W(r) = 1 - \frac{A}{4}\left[r - \left(R_c - \frac{2}{A}\right)\right] \\
&\quad \text{for} \quad R_c - \frac{2}{A} < r < R_c + \frac{2}{A}, \\
&W(r) = 0 \\
&\quad \text{for} \quad r \ge R_c + \frac{2}{A}.
\end{aligned}
\tag{13}
$$

The constant A determines the steepness of the cutoff and was chosen $A = 5$ Å^{-1}. The parameters γ_1 and γ_2 are normalization constants which correct for the larger number of atoms contributing to $\bar{n}_i$ and $\bar{n}_i^{fcc}$ if the theory is extended to interactions beyond nearest neighbours. For a cutoff between fourth- and fifth-nearest neighbours the normalization constants are $\gamma_1 = 1.04310$ and $\gamma_2 = 1.06887$ [8].

3.2. Monte Carlo simulations

Simulations were performed of Al(111) and Al(110) surfaces. The calculational unit cell consisted of a rectangular box of Al atoms. As an example we show in fig. 1 the projection of the atomic coordinates on the $(1\bar{1}0)$ plane for the cell used in simulations of Al(111) at 300 K. At the bottom of the cell six layers of atoms which were "frozen" at perfect fcc lattice positions defined the orientation of the surface. The atoms in the layers on top of the frozen layers were free to move. For the Al(111) surface each layer consisted of 30 atoms and the number of free atom layers was varied from 12 at 300 K to 18 at 850 K. For the more open Al(110) surface each layer consisted of 20 atoms and the number of free layers was varied from 12 at 300 K to 24 at 900 K. Below the free layers there were 8 (110)-layers of frozen atoms. At elevated temperatures the number of free atom layers had to be increased in order to allow the ion scattering experiment to probe deeper regions in the crystal. This was necessary because of the reduction of shadowing and blocking due to the increase in thermal vibrations and

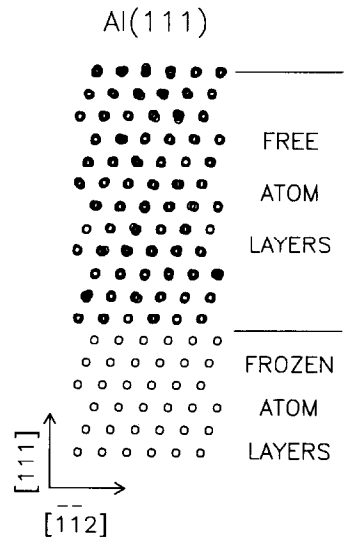

Fig. 1. Illustration of the unit cell used in the simulations of the Al(111) surface. This figure shows a typical snapshot of the atomic configuration at 300 K. The positions of the atoms are projected onto the $(1\bar{1}0)$ plane.

the (possible) presence of disorder in the surface region at high temperatures. The number of free layers was always sufficiently large that the scattering yield per layer reached its minimum-yield value at least 4 layers away from the frozen atom layers, which is the distance over which the ion scattering can be influenced significantly by the presence of the frozen atom layers. In the starting configuration at 300 K all atoms were positioned at fcc lattice sites. The lattice constant used at a given temperature to set up the fcc lattice was taken from simulations of a bulk Al crystal as described at the end of this section. For higher temperatures the starting configuration was usually obtained by expanding a cell equilibrated at a lower temperature so that the appropriate lattice constant was obtained, and adding a number of extra free atom layers if necessary. In directions parallel to the frozen atom layers periodic boundary conditions were applied. In the perpendicular direction there were no constraints except that the frozen atom layers remained fixed. The stepsize of the atom displacements in the MC simulation was adjusted to give an acceptance fraction of 50% of the attempted moves. The crystals were first equilibrated at each temperature which took typically 5000 MC cycles at 300 K and up to 50000 cycles at the highest temperatures studied, as judged from the number of cycles after which the calculated ion scattering yields did no longer change significantly. (One MC cycle is defined to consist of one attempted move for each free atom in the cell.) After equilibration "snapshots" of the crystals were generated by storing the atomic positions. The system was run 10 MC cycles between each generated snapshot in order to make them approximately independent. After the generation of 50 snapshots the system was run another 5000 MC cycles after which a truly independent next series of snapshots was obtained. Examples of snapshots are shown in fig. 2 where the positions of the atoms in the calculational unit cell are projected onto the $(1\bar{1}0)$ plane. For clarity only the 6 topmost free atom layers are shown for the Al(111) surface, and 9 layers for Al(110). At 300 K both surfaces are well-ordered as seen in the top panel of fig. 2. However, at 850 K the snapshot for the Al(110) surface shows the onset of disorder in the surface region whereas Al(111) remains ordered.

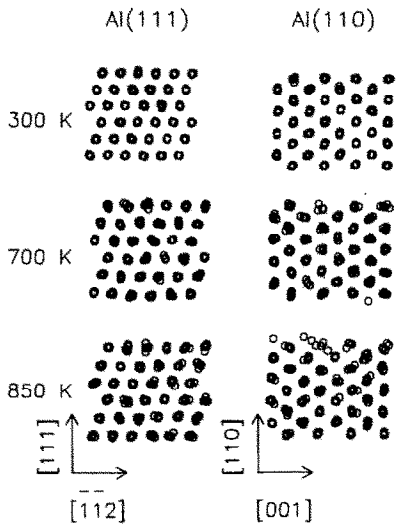

Fig. 2. Snapshots for Al(111) and Al(110) at various temperatures. The positions of the atoms are projected on the $(1\bar{1}0)$ plane. For clarity, only the topmost 6 free atom layers are shown for Al(111) and the topmost 8 for Al(110).

After generation of typically 200 snapshots we performed calculations of the scattering yield using the method described in section 2. On each snapshot a total of 100 ions Å^{-2} were tracked through the crystal, amounting to a total of ~ 22500 ions per snapshot. The influence of the parameter δ (see section 2) was investigated on snapshots of the Al(111) surface at 300 K. The bulk one-dimensional rms displacement of the atoms at 300 K as measured in the simulations was 0.102 Å. It was found that for $\delta \leq 0.05$ Å, reliable values for the scattering yields were obtained. For $\delta = 0.10$ Å the obtained scattering yields were significantly higher. This confirms the estimate made in section 2, namely that δ must be chosen small compared to the rms displacement of the atoms. In all our simulations reported in section 4 we have used $\delta = 0.05$ Å. Since the rms displacement of the atoms increases with temperature the approximation made in eq. (5) is even better at the higher temperatures.

At each temperature the bulk lattice constant has to be known accurately in order to properly determine the positions of the atoms in the start-

ing configuration and the in-plane dimensions of the unit cell. In order to avoid the presence of strain in the simulations the lattice constant must be obtained from simulations of a bulk system with precisely the same potential as used in the surface simulations. We have performed MC simulations of a bulk fcc Al crystal with the calculational unit cell consisting of a box of 108 Al atoms and with periodic boundary conditions in three orthogonal directions. In these bulk simulations the size of the unit cell was allowed to vary and thus the equilibrium lattice constant at zero external pressure was determined. For temperatures between 300 and 900 K the lattice constant was found to be $a(T) = 4.019 + 7.003 \times 10^{-4}T + 2.939 \times 10^{-7}T^2$ (Å). Our values are about 1% lower than the results in ref. [27] due to a slightly different definition of the cutoff of the interactions.

4. Results

4.1. Scattering yields from Al(111) at 300 K

The inset in fig. 3 shows the geometry used in the ion scattering experiments and simulations on Al(111). The preparation of the Al(111) surface and the experimental conditions have been described elsewhere [17]. A beam of 100 keV protons was incident along the $[\bar{1}\bar{1}0]$ direction of the Al crystal. Scattering yields were measured and calculated for protons emerging with scattering angles ranging from 80 to 100°. The resulting simulated blocking profile at 300 K is shown by the solid curve in fig. 3. Our experimental blocking profile is indicated by the open circles. The calculated scattering yields are 0.3 monolayer (ML) higher than the measured yields (1 monolayer of Al(111) corresponds to 1.41×10^{15} atoms cm^{-2}). This is most likely an artifact of the MC simulations which will be discussed in section 5.1. The dashed curve in fig. 3 shows the calculated blocking profile, shifted downwards by 0.3 ML. Clearly the shape of the blocking profile is in good agreement with the measured profile. We conclude that the EMT describes the Al(111) surface well at room temperature.

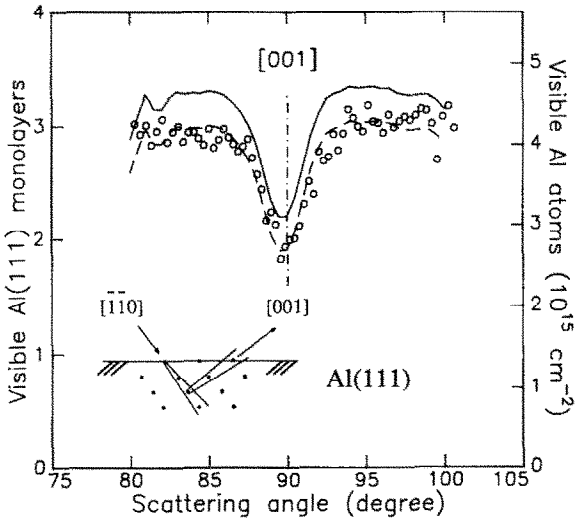

Fig. 3. Blocking profiles for the Al(111) surface at room temperature, obtained in the scattering geometry shown in the inset. The solid curve represents the result of the EMT simulations, and the dashed curve shows the same results reduced by 0.3 Al(111) monolayers. The open circles indicate the experimental scattering yields. The dashed–dotted line indicates the scattering angle for ions that have emerged from the crystal along the [001] direction.

4.2. Temperature-dependent scattering yield from Al(111)

The temperature dependence of the scattering yield from the Al(111) surface was calculated from 300 to 850 K, in the scattering geometry of fig. 3. The resulting yields for ions which leave the crystal along the [001] blocking direction are shown in fig. 4 as solid squares. Experimental yields from ref. [17] are also shown (open circles). Qualitatively, the simulated and measured scattering yields show the same temperature dependence in the temperature range studied: the yield increases almost linearly with temperature. It has previously been shown that the increase of the experimental yield with temperature can be fully attributed to the increase of the atomic vibration amplitudes with temperature. The surface remains well-ordered up to the bulk melting point. A quantitative comparison between the calculated and experimental scattering yields shows that their difference increases from 0.3 ML at 300 K (see section 4.1) to 1.4 ML at 850 K. We associate this difference with

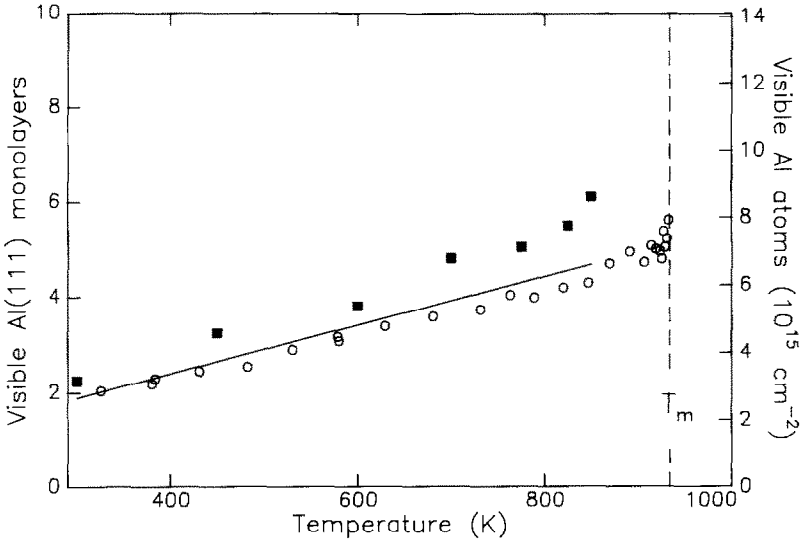

Fig. 4. Temperature dependence of the scattering yield from the Al(111) surface, obtained in the scattering geometry shown in fig. 3. The EMT results are shown by the solid squares and the experimental yields by the open circles. The solid curve is discussed in section 5.1.

a shortcoming of the MC simulations (see section 5.1) rather than an inadequacy of the EMT.

4.3. Scattering yields from Al(110) at 300 K

The scattering geometry used for the Al(110) surface is shown in the inset of fig. 5. Simulated scattering yields for 100 keV protons impinging on the crystal along the [$\bar{1}$01] direction and emerging from the crystal with scattering angles ranging from 50 to 70° are shown by the solid curve in fig. 5. The experimental results are indicated by the open circles. For the preparation of the Al(110) surface and the experimental conditions we refer to ref. [17]. The calculated scattering yields are in excellent agreement with the experiment, both in intensity and in the shape of the blocking profile. We conclude that the EMT provides an excellent description of the Al(110) surface at room temperature.

4.4. Temperature dependent scattering yield from Al(110)

Scattering yields calculated for the Al(110) surface for ions emerging from the crystal along the [011] direction (see fig. 5) are shown in fig. 6 for temperatures between 300 and 900 K (solid squares). Experimentally obtained yields are also shown (open circles [17]). The calculations are in

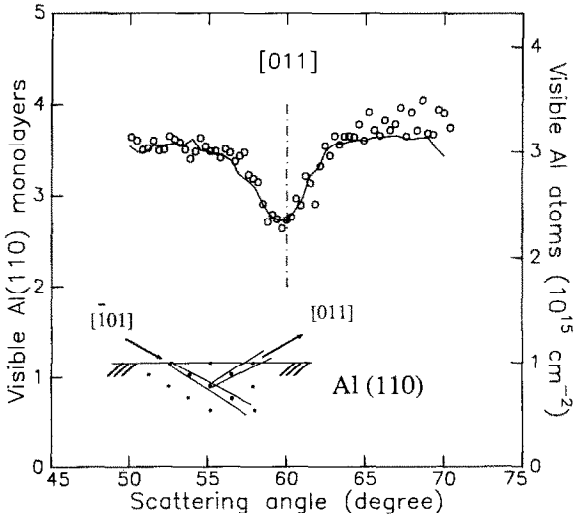

Fig. 5. Blocking profiles for the Al(110) surface at room temperature, obtained in the scattering geometry shown in the inset. Results of the EMT simulations are shown by the solid curve, and the open circles show the experimental scattering yields. The dashed–dotted line indicates the scattering angle for ions that have emerged from the crystal along the [011] direction.

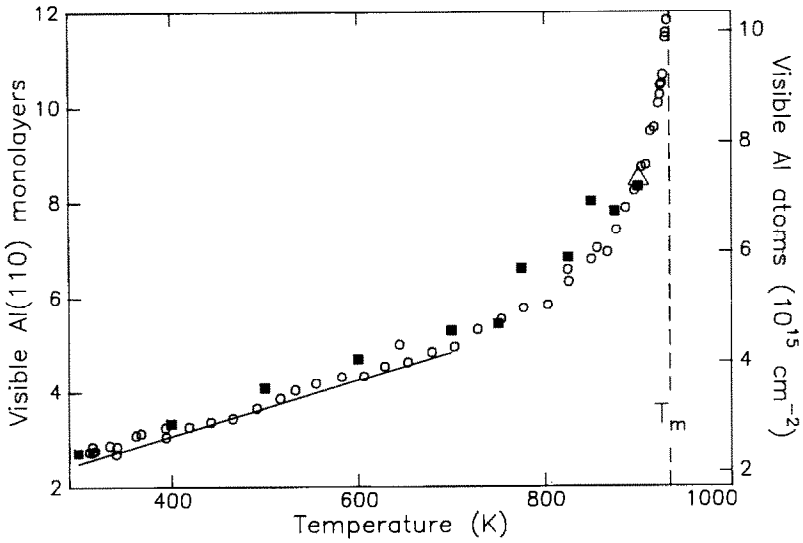

Fig. 6. Temperature dependence of the scattering yield from the Al(110) surface, obtained in the scattering geometry shown in fig. 5. Results of the EMT simulations are represented by the solid squares and the open triangle. The open circles show the experimental scattering yields. The rapid increase of the scattering yield at temperatures above 775 K indicates the onset of disorder on the Al(110) surface. The solid curve is discussed in section 5.1.

good agreement with the experiment over the entire temperature range studied: at low temperatures, from 300 to 750 K, the yield increases slowly with temperature, at a rate that is expected for an ordered Al(110) surface [17]. Above 750 K the yield increases much faster with temperature, which has been attributed before to surface melting [17]. The calculated yield follows the experimental data quite closely in this temperature regime. We conclude that the EMT provides a good description of the Al(110) surface, both in the temperature range where the surface is ordered and in the early stages of surface melting.

5. Discussion

5.1. Shortcoming of the MC simulations

We now show that the difference between the simulated and measured scattering yields on Al(111) is caused by an artifact of the simulations. In MC as well as MD simulations each of the free layers of atoms has some freedom to make correlated shifts parallel to the surface with respect to the other atom layers. Since the (shifted) layers are repeated periodically the surrounding copies of the simulation cell do not produce a restoring force against these shifts. Of course, the restoring force resulting from the interaction with the adjacent layers, above and below, remains intact. Nevertheless, the net resistance against shear fluctuations of the free layers is reduced in the simulations for wavelengths exceeding the lateral size of the simulation cell. Although the effect is small it noticeably enhances the ion scattering intensities.

The artificial increase in calculated scattering signal is estimated by the following analysis of the simulation results. We start with the structure factor $S_j(\boldsymbol{Q})$ of layer j at the in-plane reciprocal lattice vector $\boldsymbol{Q}$:

$$S_j(\boldsymbol{Q}) = \frac{1}{N_j} \sum_{l=1}^{N_j} \exp \mathrm{i}(\boldsymbol{Q} \cdot \boldsymbol{x}_l). \tag{14}$$

The summation index l runs over all N_j atoms in layer j. If the displacement distribution of the atoms from their lattice positions is approximately Gaussian we obtain the rms displacement $\sigma_j(\hat{\boldsymbol{Q}})$

of the atoms in layer j in the direction of $\hat{\boldsymbol{Q}} = \boldsymbol{Q}/|\boldsymbol{Q}|$ from

$$\sigma_j^2(\hat{\boldsymbol{Q}}) = -\frac{1}{Q^2}\ln\left[\frac{\langle|S_j(\boldsymbol{Q})|^2\rangle - \langle 1/N_j\rangle}{1-\langle 1/N_j\rangle}\right]. \tag{15}$$

Here $\langle \ldots \rangle$ denotes an average over a large number of independent configurations generated by the MC algorithm. The terms containing N_j correct for the limited number of atoms in the layer and vanish for an infinitely large system. The $\sigma_j(\hat{\boldsymbol{Q}})$ as given by eq. (15) are the rms displacements of the atoms with respect to the instantaneous centre of mass of layer j and are thus *insensitive* to shifts of the entire layer. Using eq. (15) we have determined from the EMT simulations the rms atomic displacements in the different layers of Al(111). We have also determined the rms displacements $\sigma_j^*(\hat{\boldsymbol{Q}})$ directly from the simulations, where $\sigma_j^*(\hat{\boldsymbol{Q}})$ *includes* the layer shifts. After averaging over 5000 MC configurations we find the directly measured rms displacements σ^* to be typically 20% larger than the rms displacements σ obtained from eq. (15).

That a 20% difference in rms displacement is sufficient to cause the difference between the EMT results in fig. 4 (solid squares) and the experimental data (open circles) is illustrated by the solid curve in fig. 4. The curve is the result of a calculation of the scattering yield from an ordered Al(111) surface with a conventional ion-scattering algorithm [21]. In this calculation the atoms were assumed to vibrate harmonically, corresponding to Gaussian displacement distributions around equilibrium positions, with the shift-corrected rms displacements σ_j obtained from eq. (15). The solid curve is indeed significantly lower than the result of the "full" EMT simulations and close to the experimental scattering intensities.

A similar analysis for the Al(110) surface in the temperature regime where the surface is well-ordered yields the solid curve in fig. 6, which is in excellent agreement with the experimental data. It appears that the influence of the shifts on the ion scattering yields is larger for the Al(111) surface than for the Al(110) surface. We note that for the Al(110) surface the shifts are much larger along the close-packed [1$\bar{1}$0] direction than along the open [001] direction. Along a close-packed direction the probability for a collective displacement of all atoms within one layer of the unit cell is obviously largest. This also explains why the influence of the shifts on the scattering yields is larger for Al(111) than for Al(110); the Al(111) surface contains close-packed rows in three in-plane directions, and the Al(110) surface in only one. In addition, the number of nearest neighbours an atom has in adjacent layers is larger for Al(110) than for Al(111), so that the restoring interlayer interactions are probably largest for Al(110). Care has to be taken in studying the anisotropy of surface melting in simulations of the Al(110) surface since the (anisotropic) shifting may influence the results.

The shifts are caused by the finite size of the calculational unit cell. We have performed a simulation of the Al(110) surface at 900 K with the size of the unit cell doubled in both in-plane directions. This leads to a crystal with 80 atoms per layer and a total of 1920 free atoms. The resulting values for σ_j^* are considerably lower than those for the smaller system, and are close to the values for σ_j. In addition the values of $\sigma_j^*(\hat{\boldsymbol{Q}})$ are nearly equal for the [1$\bar{1}$0] and the [001] directions, in contrast with the observed anisotropy for the smaller system. The calculated ion scattering yield from the large unit cell at 900 K is indicated by the open triangle in fig. 6. It is seen that this yield is close to that for the smaller system which confirms the observation that the layer shifts in the smaller system do not strongly influence the ion scattering yields from Al(110).

5.2. Creation of adatoms and vacancies

From the comparison between calculated and measured scattering yields presented in section 4 and from the discussion in section 5.1 we feel confident that the simulations provide a realistic description of Al surfaces. Therefore we may expect to learn about the microscopic processes occurring on these surfaces at elevated temperatures by investigating the simulation results. We now show that the onset of disorder as seen with ion scattering on the Al(110) surface is strongly corre-

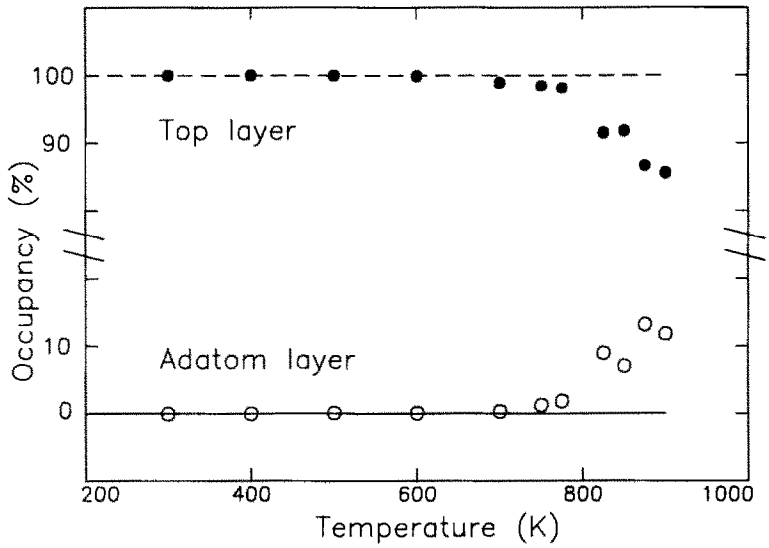

Fig. 7. The occupancy of the top layer (solid circles) and the adatom layer (open circles) as a function of temperature for the Al(110) surface. The sudden increase of the occupancy of the adatom layer at 800 K marks the formation of adatom–vacancy pairs.

lated with the production of adatoms and vacancies. In fig. 7 the occupied fraction of the top layer and the layer above (adatom layer) is plotted as a function of temperature. At low temperatures the occupied fractions of the top and adatom layers are 1 and 0, as expected for an ordered surface. For temperatures above ~ 775 K the occupied fraction of the top layer decreases and the occupied fraction of the adatom layer becomes nonzero. Atoms are moving out of the top layer into the adatom layer. This mechanism is confirmed by inspection of individual snapshots and simulated density profiles, and agrees with previous computer simulation results on surface melting [7,13]. Comparison of figs. 6 and 7 shows that the adatom–vacancy creation commences at the same temperature where ion scattering detects the onset of surface disorder. In the simulations of Al(111) it was found that adatom–vacancy pairs are absent up to at least 900 K. We conclude that the disorder seen with ion scattering is closely related to the creation of adatoms and vacancies.

It should be noted that the additional scattering yield at high temperatures for Al(110) is not due to the scattering of ions from the adatoms. At 900 K, the scattering yield from the simulated Al(110) surface is about 2 Al(110) monolayers larger than the yield expected for an ordered Al(110) surface (see fig. 6). The total density of adatoms at this temperature is less than 0.15 monolayer. Thus, the main contribution to the additional scattering yield must be ascribed to disordering of the other atoms in the top layers of the crystal. This supports the hypothesis that the creation of vacancies in the top layer allows the remaining atoms to become disordered [7].

6. Conclusions

In summary, we have presented a formalism for the calculation of ion scattering yields from simulated crystal surfaces. The results can be directly compared with experimental scattering yields. Input in the simulations are the interatomic potential of the atoms in the crystal and the interaction potential between the ions and the atoms. Since the latter potential is well known, this approach provides a quantitative test of the adequacy of the interatomic potential.

We have used the effective-medium theory to simulate Al(111) and Al(110) surfaces. The calculated ion scattering yields are in good agreement with experimentally obtained scattering yields. The

absence of surface melting on simulated Al(111) up to at least 850 K corresponds well with the experimental observations. For Al(110) we find that the simulated crystal provides an excellent description of the onset of surface melting. The simulations reveal that the onset of disorder which is detected with ion scattering is accompanied by the creation of adatoms and vacancies.

Acknowledgements

Professor Dr. J.F. van der Veen is gratefully acknowledged for many stimulating discussions during the course of this project. This work is part of the research program of the Stichting voor Fundamenteel Onderzoek der Materie (FOM) and is made possible by financial support from the Nederlandse Organisatie voor Wetenschappelijk Onderzoek (NWO). A.W.D. vd G. and P.S. gratefully acknowledge travel support from the ESF-Network in Surface Crystallography.

References

[1] F.H. Stillinger and T.A. Weber, Phys. Rev. B 31 (1985) 5262.
[2] M.H. Grabow and G.H. Gilmer, Surf. Sci. 194 (1988) 333.
[3] J.P. van der Eerden, L. Guang-zhao, F. de Jong and M.J. Anders, J. Cryst. Growth, 99 (1990) 106.
[4] J.F. Lutsko, D. Wolf, S.R. Phillpot and S. Yip, Phys. Rev. B 40 (1989) 2841.
[5] S. Iarlori, P. Carnevali, F. Ercolessi and E. Tosatti, Surf. Sci. 211/212 (1989) 55.
[6] P. Stoltze, J.K. Nørskov and U. Landman, Phys. Rev. Lett. 61 (1988) 440.
[7] P. Stoltze, J.K. Nørskov and U. Landman, Surf. Sci. 22 (1989) L693.
[8] P. Stoltze, J. Chem. Phys. 92 (1990) 6306.
[9] E.G. McRae, J.M. Landwehr, J.E. McRae, G.H. Gilmer and M.H. Grabow, Phys. Rev. B 38 (1988) 13178.
[10] J. Tallon, Phys. Rev. Lett. 57 (1986) 1328.
[11] P. Carnevali, F. Ercolessi and E. Tosatti, Phys. Rev. B 36 (1987) 6701.
[12] W. Schommers and P. von Blanckenhagen, J. Vac. Sci. Technol. A 5 (1987) 644.
[13] E.T. Chen, R.N. Barnett and U. Landman, Phys. Rev. B 41 (1990) 439.
[14] J.F. van der Veen, Surf. Sci. Rep. 5 (1985) 199.
[15] J.W.M. Frenken, P.M. Marée and J.F. van der Veen, Phys. Rev. B 34 (1986) 7506.
[16] B. Pluis, A.W. Denier van der Gon, J.W.M. Frenken and J.F. van der Veen, Phys. Rev. Lett. 59 (1987) 2678.
[17] A.W. Denier van der Gon, R.J. Smith, J.M. Gay, D.J. O'Connor and J.F. van der Veen, Surf. Sci. 227 (1990) 143.
[18] J.H. Barrett, Phys. Rev. B 3 (1971) 1527.
[19] I. Stensgaard, L.C. Feldman and P.J. Silverman, Surf. Sci. 77 (1978) 513.
[20] R.M. Tromp and J.F. van der Veen, Surf. Sci. 133 (1983) 159.
[21] J.W.M. Frenken, R.M. Tromp and J.F. van der Veen, Nucl. Instrum. Methods B 17 (1986) 334.
[22] K.W. Jacobsen, J.K. Nørskov and M.J. Puska, Phys. Rev. B 35 (1987) 7423.
[23] If an ion is deflected more than once before leaving the crystal, then the cross-section for backscattering will be slightly different from the cross-section for backscattering into the same final direction by a single scattering even. This difference is neglected in eq. (1) but is taken into account properly in our simulations [21].
[24] D.P. Jackson and J.H. Barrett, Comput. Phys. Commun. 13 (1977) 157.
[25] D.W. Heerman, Computer Simulation Methods in Theoretical Physics (Springer, Berlin, 1986).
[26] G. Molière, Z. Naturforsch. 2 A (1947) 133.
[27] P. Stoltze, K.W. Jacobsen and J.K. Nørskov, Phys. Rev. B 36 (1987) 5035.
[28] E.V. Zarochentsev, S.P. Kravchuck and T.M. Tarusina, Sov. Phys. Solid State 18 (1976) 239.